nature physics

SUPPLEMENTARY INFORMATION

DOI: 10.1038/NPHYS1276

Individual topological tunnelling events of a quantum field probed through their macroscopic consequences

Mitrabhanu Sahu[1], Myung-Ho Bae[1], Andrey Rogachev[1,2], David Pekker[1,3], Tzu-Chieh Wei[1,4], Nayana Shah[1], Paul M. Goldbart[1] & Alexey Bezryadin[1]

[1]*Department of Physics, University of Illinois at Urbana Champaign, 1110 West Green Street, Urbana, Illinois 61801, USA.*

[2]*Department of Physics, University of Utah, 115 S 1400 E, Salt Lake City, Utah 84112, USA.*

[3]*Department of Physics, Harvard University, 17 Oxford Street, Cambridge, Massachusetts 02138, USA.*

[4]*Institute for Quantum Computing and Department of Physics and Astronomy, University of Waterloo, 200 University Ave. W., Waterloo, Ontario N2L 3G1, Canada.*

This section contains:

1. **Discussion of the thermally activated phase slip (TAPS) and quantum phase slip (QPS) rates.**
2. **Heat capacity and thermal conductivity of nanowire.**
3. **Macroscopic quantum tunnelling in high-T_C intrinsic Josephson junctions.**
4. **Filtering system in our measurement setup.**
5. **Supplementary references.**

DOI: 10.1038/NPHYS1276

Discussion of the thermally activated phase slip (TAPS) and quantum phase slip (QPS) rates

To fit the low-bias R vs. T data we used the expression,

$$R(T) = \left[R_{\mathrm{LAMH}}^{-1}(T) + R_{\mathrm{N}}^{-1} \right]^{-1} \quad (1)$$

Here, we have taken into account the normal conductance channel, which is due to quasi-particles and this conductance is typically estimated as $1/R_{\mathrm{N}}$. This normal channel is connected in parallel with the conductance of the condensate in the wire (R_{LAMH}), which is not infinite due to TAPS (*1*,*2*). The theory of TAPS, developed by Langer-Ambegaokar and McCumber-Halperin, is called LAMH (*3*,*4*). According to this theory the resistance due to TAPS is given by

$$R_{LAMH}(T) = \frac{\pi\hbar^2\Omega(T)}{2e^2k_BT}\exp\left(-\frac{\Delta F(T)}{k_BT}\right) \quad (2)$$

where $\Delta F(T) = \frac{8\sqrt{2}}{3}\left(\frac{H_C^2(T)}{8\pi}\right)A\xi(T)$ is the energy barrier for phase slips,

$\Omega(T) = \left(L/\xi(T)\right)\left(\Delta F(T)/k_BT\right)^{1/2}\left(1/\tau_{GL}\right)$ is the attempt frequency,

$\tau_{\mathrm{GL}} = [\pi\hbar/8k_{\mathrm{B}}(T_{\mathrm{C}} - T)]$ is the Ginzburg-Landau (GL) relaxation time, L is the length of the wire, A is the cross-sectional area, $\xi(T)$ is the GL coherence length, $H_{\mathrm{C}}(T)$ is the critical field and T_{C} is the critical temperature of the wire. The T dependence of the of the energy barrier $\Delta F(T)$ and the attempt frequency $\Omega(T)$ come in the expression via $\xi(T)$ and $H_{\mathrm{C}}(T)$, which are given as

$$\xi(T) = \xi(0)\frac{\left(1-\left(\frac{T}{T_C}\right)^4\right)^{0.5}}{\left(1-\left(\frac{T}{T_C}\right)^2\right)} \quad (3)$$

$$H_C(T) = H_C(0)\left[1.73\left(1-\frac{T}{T_C}\right)-0.40087\left(1-\frac{T}{T_C}\right)^2-0.33844\left(1-\frac{T}{T_C}\right)^3+0.00722\left(1-\frac{T}{T_C}\right)^4\right] \quad (4)$$

Here we have found the temperature dependence of $H_C(T)$ by fitting the numerical tabulation given by Muhlschlegel to a polynomial fit (*2,5*) applicable at all temperatures below T_C. Also, the energy barrier at zero temperature $\Delta F(0)$ can be expressed in terms of wire parameters (*6*),

$$\Delta F(0) = \frac{1.76\sqrt{2}}{3}\left(\frac{R_Q}{R_N}\right)\left(\frac{L}{\xi(0)}\right)k_B T_C \quad (5)$$

where $R_Q = h/4e^2 \approx 6.45\text{k}\Omega$. The fitting parameters are T_C and $\xi(0)$. The length L of the wire is determined from SEM images. The normal resistance R_N of the wire is taken to be resistance measured as the film electrodes, connected in series with the wire, become superconducting.

Alternatively, one can express the free energy barrier in terms of the critical depairing current $I_C(T)$ (*6,7,8,9*) as, $\Delta F(T) = \frac{\sqrt{6}\hbar I_C(T)}{2e}$, where,

$I_C(T) = (92uA)\frac{LT_C}{R_N\xi(0)}\left(1-\left(\frac{T}{T_C}\right)^2\right)^{3/2}$ (where, L and $\xi(0)$ are in nm, T_C is in K and R_N is in Ω). A more useful expression directly applicable for our high-bias measurements

DOI: 10.1038/NPHYS1276

data, which takes into account both the temperature and bias-current dependence of the energy barrier $\Delta F(T,I)$, is given by (*7,8*),

$$\Delta F(T,I) = \frac{\sqrt{6}\hbar I_C(T)}{2e}\left(1-\frac{I}{I_C}\right)^{5/4} \tag{6}$$

The TAPS rate, Γ_{TAPS} used in the overheating model is given by,

$$\begin{aligned}\Gamma_{TAPS} &= \left(\frac{\Omega_{TAPS}}{2\pi}\right)\exp\left(-\frac{\Delta F(T,I)}{k_B T}\right) \\ &= \left(\frac{1}{2\pi}\right)\left(\frac{L}{\xi(T)}\right)\left(\frac{1}{\tau_{GL}}\right)\left(\frac{\Delta F(T)}{k_B T}\right)^{1/2}\exp\left(-\frac{\Delta F(T,I)}{k_B T}\right)\end{aligned} \tag{7}$$

A simple model of quantum phase slips was suggested by Giordano (*10*). We use this model, but instead of the Ginzburg-Landau relaxation time, which is only correct near T_C, we use the notion of the effective "quantum" temperature T_{QPS}, which is a common (and well-tested) approach in Josephson junctions (JJ) (*11*). Thus, the QPS rate, Γ_{QPS} is given by,

$$\begin{aligned}\Gamma_{QPS} &= \left(\frac{\Omega_{QPS}}{2\pi}\right)\exp\left(-\frac{\Delta F(T,I)}{k_B T_{QPS}}\right) \\ &= \left(\frac{1}{2\pi}\right)\left(\frac{L}{\xi(T)}\right)\left(\frac{1}{\tau_{GL}}\right)\left(\frac{\Delta F(T)}{k_B T_{QPS}}\right)^{1/2}\exp\left(-\frac{\Delta F(T,I)}{k_B T_{QPS}}\right)\end{aligned} \tag{8}$$

Here, T_{QPS} is the effective quantum temperature representing the strength of zero-point fluctuations in the *LC*-circuit formed by the nanowire, which has a nonzero kinetic inductance of the order of 0.1 nH, and the leads, with a mutual capacitance of the order of 1-10 fF. Thus we can roughly estimate the plasma frequency as $1/\sqrt{LC}$ and

therefore the expected quantum temperature is $\hbar / 2\pi k_B \sqrt{LC} \sim 1$ K. Experimentally we indeed find that the quantum temperature is of the order of 1 K. We also note that that to obtain a good agreement between the experimental switching rate and the quantum model a week linear dependence of T_{QPS} on the bath temperature T has to be assumed (see Fig. 4c). More precisely, we use $T_{QPS}(T) = 0.726 + 0.40 \times T$ (in Kelvins) for sample S1. For all the TAPS and QPS rates the wire parameters [i.e., R_N, L, T_C, and $\xi(0)$] are kept the same. For example, for sample S1, R_N = 2666 Ω, L = 110 nm, T_C = 3.872 K and $\xi(0)$ = 5.038 nm.

Furthermore, we find that below a crossover temperature T^*, the QPS rate dominates over the TAPS rate, i.e., quantum fluctuations dominate over the thermally induced fluctuations. For sample S1, T^* = 1.21 K (see Fig. 4c). Similar analysis on another four nanowires (S2-S5) reveals that the crossover temperature decreases with decreasing critical depairing current; as shown in Fig. 4c. This is an important fact since it leads to a conclusion that the observed QPS effect, i.e., the observation of T_{QPS} to be higher than the bath temperature, is not due to some noise or weak links in the wires. This analysis is analogous to the discussion of macroscopic quantum tunnelling in JJ (see ref. 2, Fig.7.4 (page 263) in the paragraph about MQT). This increase of the T^* with the critical current indicates that the observed large value of the width of the switching current distributions is an intrinsic property of the nanowires, occurring due to QPS. In the following table, we enlist the wire parameters that were used for all the four samples to get Γ_{TAPS} and Γ_{QPS} and their form of $T_{QPS}(T)$.

We would like to mention that we discovered two data points (out of a total of 10,000 points for T = 0.9 K) and one data point (out of a total of 10,000 points for

DOI: 10.1038/NPHYS1276

T = 1 K) that have anomalously low values of switching current (with more than 30 standard deviations). For example, at T = 0.9 K the mean value of the switching current was 4.67 μA, the standard deviation was 0.04 μA, and the points that we term anomalous correspond to switching currents of 2.66 μA and 3.35 μA. It seems to us highly likely that these three points are due to factors extrinsic to our measurement setup. It is precisely these anomalous data points that cause the bump in the standard deviation for sample S5 plotted in the inset of Fig. 2. If we remove these points, the resulting curve no longer exhibits the bump. We emphasize that these anomalous points and the corresponding bump in the standard deviation versus temperature graph have no consequences on our conclusions: namely the dependence of the effective quantum-fluctuation temperature T_{QPS} on bath temperature T. Our fits for T_{QPS} (T) are linear by definition. These anomalous points are outside the range of our fitting to the switching rates for the two temperatures.

Table 1| Nanowire sample parameters, $T_{QPS}(T)$ and T^* for all samples

Nanowire Sample	L (nm)	R_N (Ω)	T_C (K)	ξ(0) (nm)	$I_C(0)$ (nA)	A (nm^2)	$T_{QPS}(T)$ (In the form a+bT) (K)	T* (K)
S1	110	2666	3.872	5.038	2917	74.2	0.726+0.40T	1.210
S2	195	4100	3.810	9.650	1727	85.6	0.404+0.362T	0.633
S3	104	1430	3.160	12.560	1683	130.9	0.199+0.678T	0.620
S4	200	3900	2.870	12.250	1105	92.3	0.275+0.33T	0.410
S5	120	1450	4.55	5.6366	6164	148.9	1.834	1.834

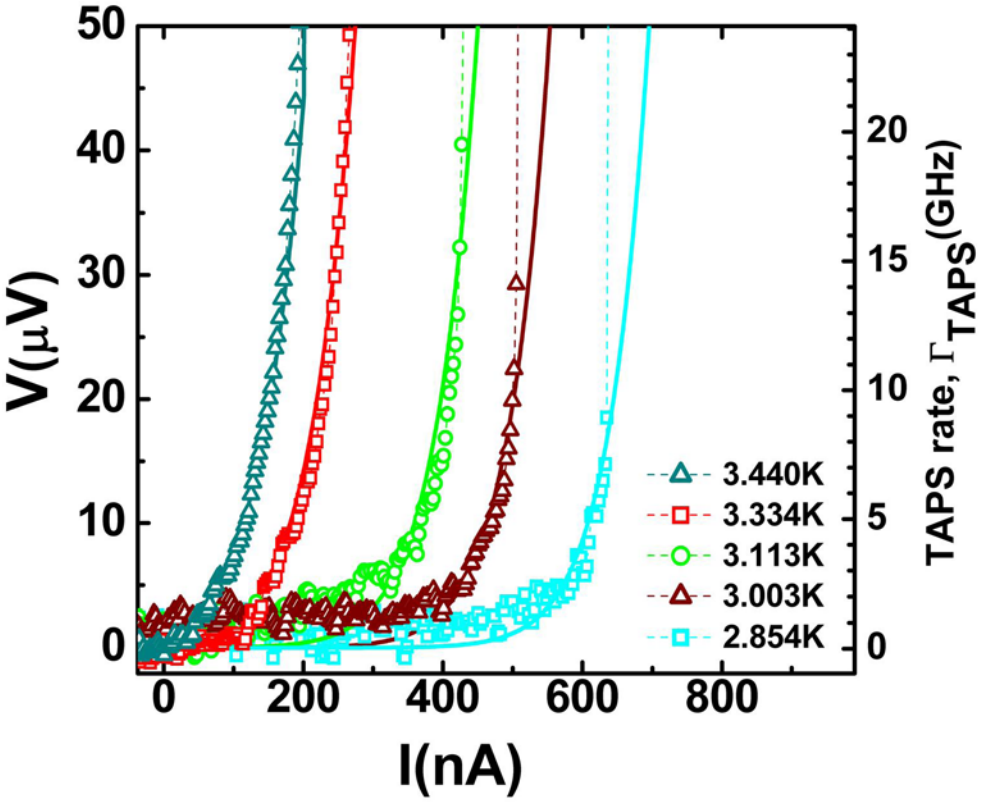

FIG. S1: High-bias V-I measurements at high temperatures where the voltage due to phase diffusion is measurable even before the switching event. The solid lines are predictions of phase slip rate using the TAPS model with the wire parameters used are those which were obtained by fitting the switching rates measurements between T = 0.3 K to 2.3 K. The phase-slip rate Γ_{TAPS} (shown in the right axis) is converted into voltage using the relation, $V = h\Gamma_{TAPS}/(2e)$. The dashed line is the line connecting the data points, not a fit.

Another independent validation of the TAPS model, applied at higher temperatures, and the wire parameters used, can be obtained from non-linear *I-V* curves measured at relatively high temperatures. At these temperatures measured *I-V* curves show tails due to TAPS that are large enough to be measured in our set up; as shown in Fig. S1 (see also Fig. 1c). In Fig. S1, we also plotted the predicted voltage obtained

DOI: 10.1038/NPHYS1276

from the TAPS model, using $V = h\Gamma_{\mathrm{TAPS}} / (2e)$. For the TAPS rate calculations, the wire parameters used for all our fittings (as shown in Fig. 3) are kept the same and only the T was varied to get the corresponding TAPS rate. The measured voltage (or phase-slip rate) and the predicted voltage (or the TAPS rate) are in good agreement for the five temperatures noted in Fig. S1. This agreement indeed verifies our model for TAPS. The calculation of the TAPS V-I curve is made under the assumption that the wire temperature equals the bath temperature, i.e., no significant Joule heating occurs. These type of phase diffusion "tails" on the V-I curves can only be seen at temperature of about 2.7 K or larger, which is about 10 times higher a temperature than those where the QPS effects are found.

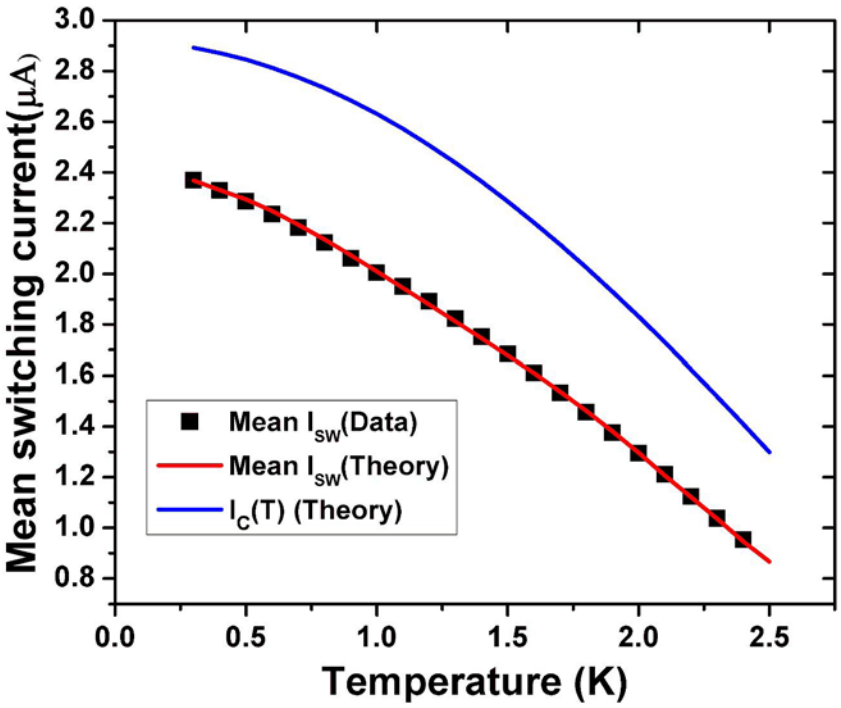

FIG. S2: The measured mean switching current (squares) and the predicted mean switching current by our model (red line) as a function of temperature. The predicted fluctuation-free critical depairing current, $I_c(T)$ is shown (blue

line). At all temperatures a premature switching occurs before the bias current reaches the critical depairing current.

The mean switching current predicted at each temperature by the overheating model and the mean switching current for each distribution (Mean I_{SW}) is compared in Fig. S2. We have also plotted the critical depairing current $I_C(T) = I_C(0)\left[1-\left(T/T_C\right)^2\right]^{3/2}$ (9). We find that at all temperatures the switching is premature.

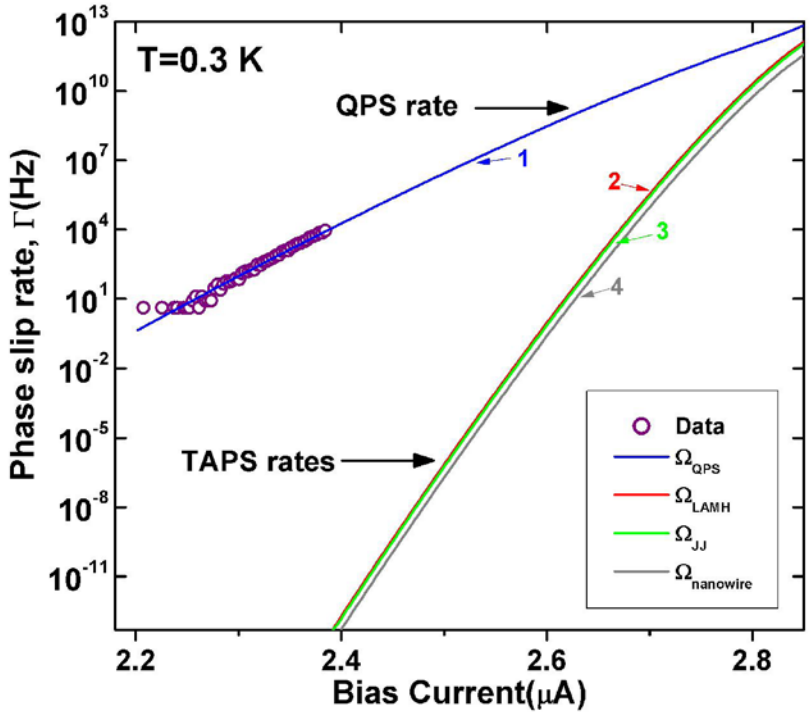

FIG. S3: The data (open circles) and the calculated QPS rate (solid blue line) at 0.3 K for wire S1. The observed agreement is very good. Different estimates of TAPS rate by using different attempt frequency expressions are also shown by solid red, green, and grey lines. For all our estimates of TAPS rate, the data is at least ~ 10^{15} orders of magnitude higher than the predicted thermal rate.

DOI: 10.1038/NPHYS1276

Hence, the data can not be explained by considering thermal fluctuation alone, even if the uncertainty in the attempt frequency is taken into account. Note also that for the lowest bias current of 2.2 μA, the thermal rate is about 10^{25} orders lower than the experimental rate, which further proves our point.

We would like to briefly comment on the attempt frequency Ω, that is used to get the TAPS rate. In Fig. S3, we have plotted the TAPS rates estimated using different expressions for Ω (curves 2 - 4), the data (open circles) and the QPS rate (curve 1) (all at 0.3 K). For curve 2 we have used, $\Omega = \left(L/\xi(T)\right)\left(\Delta F/k_B T\right)^{1/2}\left(1/\tau_{GL}\right)$ according to McCumber and Halperin expression (eq. 7), based on time-dependent Ginzburg-Landau equations. In this expression, $L/\xi(T)$ is of the order of ~ 10, $\left(\Delta F/k_B T\right)^{1/2}$ is of the order of ~ 10 and $\left(1/\tau_{GL}\right)$ is of the order of ~ 10^{12}. Hence $\left(1/\tau_{GL}\right)$ is the dominant term in the expression for Ω. We also attempt to obtain the estimates of the thermal phase slip rate without relaying on time-dependent Ginzburg-Landau equations, and arrive practically at the same conclusions, as is explained in detail below.

For curve 4, we have replaced $\left(1/\tau_{GL}\right)$ by the characteristic frequency of the nanowire, which acts as an inductor and forms an *LC*-circuit with the leads, which are coupled to each other by a capacitance. In other words, we replace $\left(1/\tau_{GL}\right)$ with $\omega_0 = 1/\sqrt{L_w C}$, where $L_w \approx \hbar L/3\sqrt{3}eI_C(T)\xi(T)$ is the kinetic inductance of the wire (*12*), and *C* is the capacitance of the leads. For the calculations *C* is taken to be 10 fF (*13*). Thus obtained curve (grey line in Fig. S3) is very close to the traditional LAMH result (the red curve). In another attempt to verify the approximate validity of the McCumber-Halperin attempt frequency, we replaced $\left(1/\tau_{GL}\right)$ by a well-known

expression of plasma frequency for a JJ (*2*), i.e., $\omega_p = \sqrt{2eI_C(T)/\hbar C}$. Again, the obtained curve 3 (the green line in Fig. S3) appears very close to the LAMH result. Thus, in all cases, we find that with the TAPS model, the prediction of the phase slip rate is ~ 10^{15} orders of magnitude smaller than the data and we can in no way account for this difference by changing the attempt frequency. Hence, it strongly indicates that, at low temperatures, the measured phase slips are QPS, not TAPS.

We can also estimate the zero-bias resistance from our high-bias switching current measurements for very low temperatures, by an extrapolation. Using eq. 2, we can convert the zero-bias phase slip rate, $\Omega(T)\exp\left(-\frac{\Delta F(T)}{k_B T}\right)$ to resistance. We find that the resistance drops exponentially from 10^{-50} to 10^{-80} Ω for temperatures from 1.1 K to 0.3 K in the QPS dominated regime. This resistance is obviously very small to be measured in a typical lab setup and can only be estimated from such an extrapolation of the switching current measurements data. We verified that this resistance is of the same order as predicted by Golubev-Zaikin (GZ) theory (*14*), which gives for zero-temperature limit the result as follows, $R_{QPS} = \Omega(T)\exp(-AR_Q L / R_N \xi(0))$. To get the resistance value of 10^{-50} to 10^{-80} Ω we varied A from 2.7 to 4.0 for T = 1.1 K to T = 0.3 K. This is in agreement with the GZ theory, since they predict that A should be of the order of unity, which we confirm.

Heat capacity and thermal conductivity of nanowire

We will briefly outline the form of C_V and K_S that were used in the overheating model to get the switching rates from the phase slip rates at different temperatures. The diameters of the wires used in our experiments are comparable to ξ_0. Thus, the

DOI: 10.1038/NPHYS1276

thermodynamic properties of these wires should be somewhere between a bulk superconductor and a normal metal. Therefore, for the purpose of computing the thermodynamic functions we model the wire as being composed of a BCS superconducting wire with cross-section A_1 in parallel to a normal metal wire with cross-section A_2.

The BCS and Fermi liquid expressions for heat capacity are

$$C_{v,BCS} = -\frac{2N_0}{T}\int E_k \frac{df_k}{d(\beta E_k)}\left(E_k + \beta\frac{dE_k}{d\beta}\right)d\xi_k, \tag{9}$$

$$C_{v,FL} = \frac{2}{3}\pi^2 N_0 k_B^2 T, \tag{10}$$

where $\beta = 1/k_B\Theta$ (with $\Theta(x) \equiv \Theta$ is the temperature at position x along the length of the wire), $E_k = \sqrt{\xi_k^2 + \Delta^2(\Theta)}$, f_k is Fermi function and $\Delta(\Theta)$ is obtained from BCS gap equation. Thus the total heat capacity of the wire is,

$$C_v = \frac{A_1 C_{v,BCS} + A_2 C_{v,FL}}{A_1 + A_2} \tag{11}$$

Similarly, the dirty limit BCS and Fermi liquid expressions for the thermal conductivity are,

$$K_{s,\mathrm{BCS}}(\Theta) = 2N_0 D\int_\Delta^\infty \frac{\mathrm{sech}^2\left[\frac{\bullet}{2k_B\Theta}\right]}{2k_B\Theta}\frac{\bullet^2}{k_B\Theta}d\bullet\bullet, \tag{12}$$

$$K_{s,\mathrm{FL}}(\Theta) = \frac{L_0\Theta L}{AR_n}, \tag{13}$$

where D is the diffusion constant (for MoGe $D \sim 1\text{cm}^2/\text{s}$), and $L_0 = \pi^2 k_B^2 / 3e^2$. The total heat conductivity is

$$K_s = \frac{A_1 K_{s,BCS} + A_2 K_{s,FL}}{A_1 + A_2} \qquad (14)$$

The fitting parameters describing heat capacity and heat conductivity are the cross-sections A_1 and A_2, and the T_C of the nanowire.

Macroscopic quantum tunnelling in high-T_C intrinsic Josephson junctions

In order to verify that we can observe MQT in our ^{3}He setup, we measured two high-T_C crystal samples with intrinsic Josephson junctions (IJJ), using the same measurement scheme that was used for the nanowire sample measurements. The general idea in doing this was that the MQT in high-T_C stacked junctions is well known and well understood. By observing the results seen by other groups we hope to gain extra confidence in the correctness of our setup. Indeed, the results obtained in such test confirm that the setup is working properly, as is explained in more details below.

DOI: 10.1038/NPHYS1276

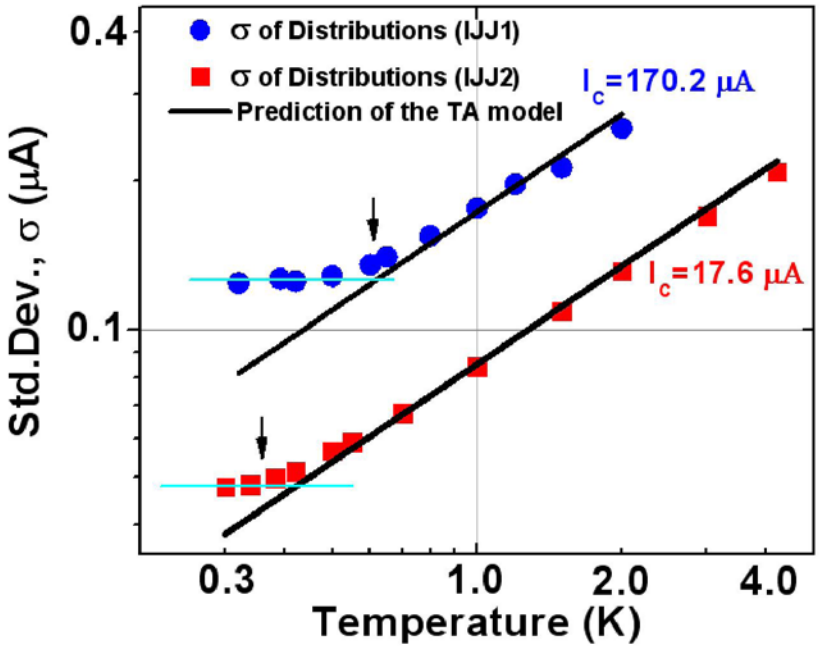

FIG. S4: Standard deviation (σ) of switching current distributions vs. temperature for two high-*T*c crystal with intrinsic Josephson junction samples (IJJ1 and IJJ2), measured in the same ^{3}He system in which all the nanowire samples were measured. We clearly see the MQT regime (denoted by the saturation of the distribution width) below a crossover temperature T^* = 0.65 K for IJJ1 and T^* = 0.35 K for IJJ2 (indicated by the two arrows). In the high temperature range, as predicted by the thermal activation model, σ is proportional to $T^{2/3}$ (solid black line). The fluctuation free critical currents for the samples are 170.2 μA (IJJ1) and 17.6 μA (IJJ2).

Fig. S4 shows the standard deviation of the switching current distributions as a function of temperature obtained from the two samples, IJJ1 and IJJ2. The samples were fabricated from $Bi_2Sr_2CaCu_2O_{8+x}$ crystal shaped using focused ion beam (FIB) to the lateral dimensions of 1.6 × 2.4 μm^2 (IJJ1). The bias current in these measurements

was injected parallel to the c-axis (i.e., perpendicular to the weakly coupled superconducting planes of the crystal). In Fig. S4, we observe a crossover from a thermal activated escape regime to MQT regime near $T^* = 0.65$ K for IJJ1 and near $T^* = 0.35$ K for IJJ2, which is manifested by a saturation behaviour of the standard deviation at lowering temperatures (*15*). We also find that, in the high temperature range, σ is proportional to $T^{2/3}$ which is expected for a thermally activated escape model (*16*). To validate this further, we estimated the escape temperature, T_{esc} , from the escape rates, Γ (obtained from switching current distributions) at different temperatures (see Fig. S5 a). For this, we used the usual expression, $\Gamma = (\omega_p / 2\pi)\exp(-\Delta U / k_B T_{esc})$, where ω_p is the plasma frequency and $\Delta U = \left(4\sqrt{2} I_0 \Phi_0 / 6\pi\right)\left(1 - I / I_0\right)^{3/2}$ (I_0 is the fluctuation free critical current) the barrier energy for escape of the "phase particle"(*11*). The obtained T_{esc} is plotted versus the bath temperature, T_{bath} in Fig. S5 b. We find that, for, high temperatures, $T_{esc} = T_{bath}$, indicating the escape process is dominated by thermal activation. For $T_{bath} < 0.65$ K, T_{esc} saturated to a value of 0.73 K, indicating a region where escape process is dominated by MQT (*11*).

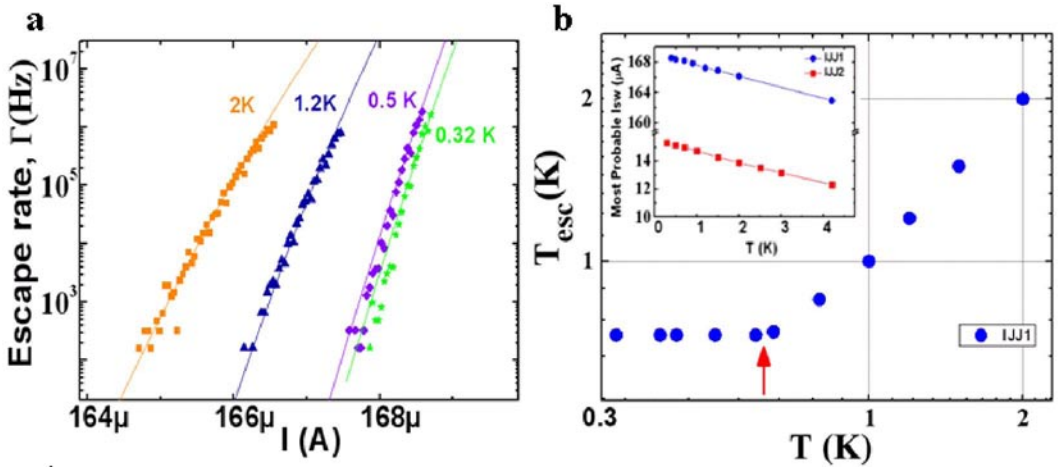

Fig. S5: a, Switching rates obtained from the switching current distributions (symbols) and the fits obtained (solid lines) using the expression

DOI: 10.1038/NPHYS1276

$\Gamma = (\omega_p / 2\pi)\exp(-\Delta U / k_B T_{esc})$ for sample IJJ1 (see text). **b,** The escape temperature T_{esc} obtained at various bath temperatures. T_{esc} saturates below ~ 0.65 K (indicated by the arrow). The inset shows the most probable switching currents for the two samples obtained from switching current distributions. The critical current for IJJ1 is ~ 10 times larger than IJJ2.

Furthermore, to verify that the saturation in σ is not due to noise (i.e., the electronic temperature not decreasing below 0.6 K), we measured another sample (IJJ2) with a critical current ~ 10 times smaller than IJJ1 ($I_C(0)$ for IJJ1 ~170.2 μA, $I_C(0)$ for IJJ2 ~17.6 μA). As shown in Fig. S4, the σ follows the prediction of the thermal activation to a lower crossover temperature of ~ 0.35 K, as is expected for a sample with a lower critical current (since the crossover temperature is proportional to $\sqrt{I_C / C}$ where I_C is the critical current and C is the junction capacitance) (*15*). Also, for both the samples, the most probable switching current increases with temperature decreasing, indicating that the sample temperature decreases with the bath temperature, down to the lowest attainable temperature (see the inset of Fig. S5 b).

The observation of crossover temperature (i.e., the observation of MQT) in high-*T*c crystals with weakly coupled superconducting planes indicates that the unexpected behaviour in σ(T) of a superconducting nanowire is not due to some uncontrolled environmental noise but originates from an intrinsic quantum fluctuations in these samples.

Filtering system in our measurement setup:

In this section we discuss the arrangement of RF filters in our ^{3}He measurement setup. The purpose of these filters is to suppress external high-frequency

electromagnetic noise, such as the noise originating from cell-phones, radio stations, and also the black-body radiation, which can, if filters are not installed, propagate through the measurement leads and reach the sample and modify the switching current observed in the experiment. Our filters are designed to reduce this noise effect to a negligible level.

Our main filtering stage is a Copper powder filter thermalized at the base temperature (0.29 K). The filter is of the type developed by Martinis, Devoret and Clarke (*11*). More details are presented below.

In our system, each signal line has three stages of filtering in series, namely, a π-filter at room temperature and a copper-powder filter (Cu-F) (at the base temperature) and silver-paste filter (Ag-F) (also, at the base temperature). These filters are necessary to suppress noise ranging from low frequency to high microwave frequencies. The compact powder filters (i.e., Cu-F or Ag-F) rely on the skin effect damping for attenuation of high frequencies. At room temperature, commercially available π-filters (Spectrum Control, SCI 1201-066) are placed on each electrical lead before they enter the cryostat. The π-filters are mounted inside an aluminium box (Hammond Manufacturing) which is attached to the top of the cryostat. The π-filters used are low-pass filters with a rated 7 dB cut-off frequency of 3 MHz. As shown in Fig. S6, for frequencies larger than 10 MHz, the measured attenuation of these π-filters is more than 20 dB. Our copper powder filters are fabricated using three feet of coiled insulated Constantan wire [Cu(55 %)Ni(45 %) alloy, resistance 18.4 Ω/feet, diameter 0.004 inch] embedded in a mixture of copper powder (-325 mesh, Alfa Aesar) and epoxy (Stycast # 1226, Emerson and Cuming). Similarly, the silver paste filters are fabricated using three feet of coiled insulated Constantan wire (the same wire) in silver paste (Fast

DOI: 10.1038/NPHYS1276

drying silver paint, Ted Pella Inc.). By measuring the signal lines with all the filters, using a vector network analyzer (Agilent N5230A), we found the attenuation to be larger that 100 dB for frequencies higher than 1 GHz. Any frequency above 6.25 GHz (which corresponds to a temperature of 0.3 K) is attenuated by more than 110 dB and falls below the noise floor of our network analyzer. This level of attenuation is similar to the attenuation used in previous experiments on MQT, see for example, ref. 11. In addition, the test performed on wires with different critical currents and on high-*T*c samples with different critical currents indicate that MQT becomes dominant at higher temperatures in samples with higher critical currents. This is a good proof of the fact that the observed behaviour is really due to MQT and not due to a noisy environment. For the corresponding discussion see ref. 2, page 262.

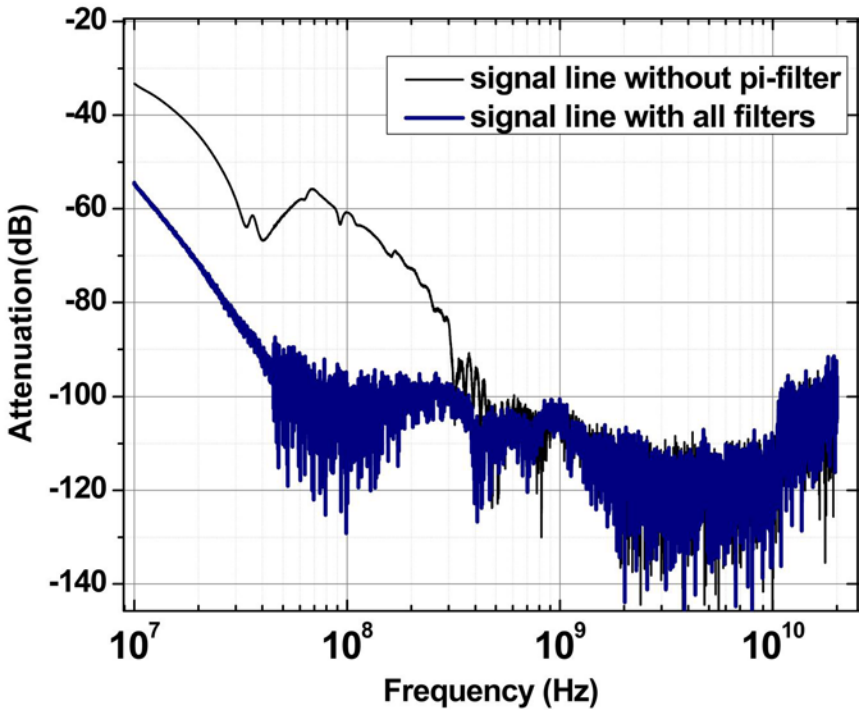

FIG. S6: Attenuation of a signal line of our ^{3}He setup measured at room temperature between 10 MHz and 20 GHz. For measurement of the signal line with all the three stages of filters (blue curve) we find attenuation larger than

90 dB for frequencies higher than 40 MHz. For frequencies higher than 6 GHz (roughly corresponding to our base temperature of $T \sim 0.29$ K), we find the attenuation to be larger than 110 dB and the signal falls below the noise level of our network analyzer. The attenuation of the signal lines without the π-filter is also shown (black curve). The π-filters provide an attenuation of 20 dB for frequencies larger than 10 MHz (rated 7 dB cut-off frequency of 3 MHz).

Supplementary References:

[1] Lau, C. N., Markovic, N., Bockrath, M., Bezryadin, A. & Tinkham, M. Quantum phase slips in superconducting nanowires. *Phys. Rev. Lett*. **87,** 217003 (2001).

[2] Tinkham, M. *Introduction to Superconductivity* 2nd edn, Ch. 8 (McGraw-Hill, New York, 1996).

[3] Langer, J. S. & Ambegaokar, V. Intrinsic resistive transition in narrow superconducting channels. *Phys. Rev.* **164**, 498–510 (1967).

[4] McCumber, D. E. & Halperin, B. I. Time scale of intrinsic resistive fluctuations in thin superconducting wires. *Phys. Rev. B* **1,** 1054-1070 (1970).

[5] Muhlschlegel, B. Die thermodynamischen funktionen des supraleiters. *Z. Phys*. **155***,* 313 (1959).

[6] Tinkham, M. & Lau, C. N. Quantum limit to phase coherence in thin superconducting wires. *Appl. Phys. Lett*. **80,** 80, 2946-2948 (2002).

[7] Tinkham, M., Free, J.U., Lau, C.N. & Markovic, N. Hysteretic I-V curves of superconducting nanowires.*Phys. Rev. B* **68**, 134515 (2003).

[8] Langer, J. S. & Ambegaokar, V. Intrinsic resistive transition in narrow superconducting channels. *Phys. Rev.* **164,** 498–510 (1967).

[9] Bardeen, J. Critical fields and currents in superconductors. *Rev. Mod. Phys*. **34,** 667–681 (1962).

[10] Giordano, N. Evidence for macroscopic quantum tunneling in one-dimensional superconductors*. Phys. Rev. Lett.* **61,** 2137 (1988).

DOI: 10.1038/NPHYS1276

[11] Martinis, J. M., Devoret, M. H. & Clarke, J. Experimental tests for the quantum behavior of a macroscopic degree of freedom: the phase difference across a Josephson junction. *Phys. Rev. B* **35,** 4682 (1987).

[12] Likharev, K.K. Superconducting weak links. *Rev. Mod. Phys.* **51,** 101-159 (1979).

[13] Bollinger, A.T., Rogachev, A. & Bezryadin A. Dichotomy in short superconducting nanowires: thermal phase slippage vs. coulomb blockade. *Europhys. Lett.* **76,** 505 (2006).

[14] Golubev, D.S. & Zaikin, A.D. Quantum tunnelling of the order parameter in superconducting nanowires. *Phys. Rev. B* **64**, 014504 (2001).

[15] Inomata, K et al. Macroscopic quantum tunneling in a *d*-wave high-T_C $Bi_2Sr_2CaCu_2O_{8+\delta}$ superconductor. *Phys. Rev. Lett.* **95,** 107005 (2005).

[16] Wallraff, A et al. Quantum dynamics of a single vortex. *Nature* **425,** 155-158 (2003).